Upper Mass-Loss Limits and Clumping in the Intermediate and Outer Wind Regions of Galactic OB stars.

M. M. Rubio-Díez[1, 2], J. O. Sundqvist[3], F. Najarro[2] , A. Traficante[4], J. Puls[5] , Calzoletti[6], D. Figer[7]

[1] Universidad de Alcalá, Madrid (Spain), [2]Centro de Astrobiología, CSIC-INTA, Madrid (Spain), [3]KU Leuven, Instituut voor Sterrenkunde, Leuven (Belgium), [4]INAF, Observatorio Astronomico di Roma, Rome (Italy), [5]Universitäts-Sternwarte München, München (Germany), [6]European Space Astronomy Center, ESA-ESAC, Madrid (Spain), [7]Rochester Institute of Technology, New York (USA)

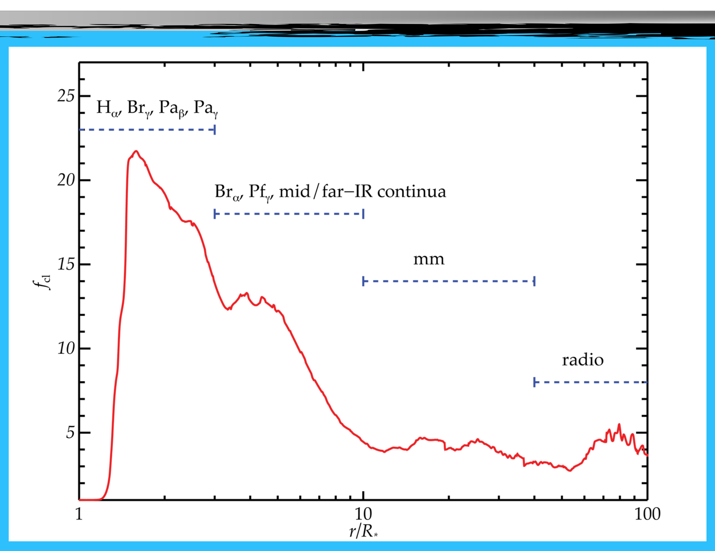

Figure 1. Radial stratification of the clumping factor for a typical O supergiant, as predicted by Sundqvist & Owocki (2013) including limb-darkening effects. The formation regions for different diagnostics are indicated.

Context.-

Mass loss is a key parameter throughout the evolution of massive stars, and it determines the feedback with the surrounding interstellar medium. The presence of inhomogeneities in stellar winds (clumping) leads to severe discrepancies not only among different mass-loss rate diagnostics (Fullerton et al. 2006, Cohen et al. 2010, Sundqvist et al. 2011), but also between empirical estimates and theoretical predictions.

The varying properties of inhomogeneities through the wind

Hydrodynamical wind simulations have shown that the presence of strong instabilities in the line-driven wind leads to formation of small-scale regions of very high densities (Owocki et al. 1988, Feldmeier 1995), which changes the structure of the atmosphere and wind. Dense 'wind clumps' can be described using either the fractional volume of dense gas, the volume filling factor (f_v, Abbott et al. 1981), or via a clumping factor (f_{cl}, Owocki et al. 1988). f_{cl} describes the overdensity of the clumps, $f_{cl} = <\rho^2> / <\rho>^2 \geq 1$, where $\langle\rho^2\rangle$ and $\langle\rho\rangle^2$ are the mean of the squared density and the mean density of gas ($\langle\rho\rangle = \dot{M}/4\pi r^2 v$) squared, respectively. Moreover, time-dependent simulations further show that the clumping factor across the wind is not homogeneous, but it presents radial stratification, $f_{cl} = f_{cl}(r)$, where r is the radial distance to the photosphere (Fig. 1). Empirically, this means that clumping differently affects the spectral diagnostic used to derive wind parameters (see review Puls et al 2008): for a given mass-loss rate, $\dot{M}$, assuming optically thin clumps, it leaves unaltered diagnostic X-ray lines, electron- scattering wings, and scattering resonance lines (ρ - dependent; e.g. C IV, P V), whereas it causes an opacity enhancement of recombination lines or free-free continuum (ρ^2- dependent; e.g. H$_\alpha$, Br$_\alpha$, mid- and far-infrared, and radio continua).

Aims.-

We aim to probe the radial clumping stratification of galactic OB stars in the intermediate and outer wind regions ($r \gtrsim 2R_\star$) to derive upper limits for mass-loss rates and to compare these to the existing mass-loss rate recipes usually used in evolutionary tracks (Vink et al. 2000,Vink et al. 2001; hereafter V00 and V01). Our sample includes 3 O giants, 2 OB dwarfs, 7 O supergiants and 13 B supergiants. This represents a unique opportunity to test theoretical mass-loss predictions for B supergiants across the so-called bi-stability jump. Since the quantitative mass-loss rates across this jump are critical for stellar evolution modelling (e.g. Vink et al. 2010, Keszthelyi et al. 2017), this has a rather important impact also on our general knowledge about the massive-star life cycle.

Methods.-

Together with archival optical to radio observations, we obtained new far-infrared continuum observations (Herschel/PACS 70, 100 and 160 micron) for our sample, which uniquely constrain the clumping properties of the intermediate wind region. We follow clumping parametrization (f_{cl}^{in} [r_{in}, r_{mid}], f_{cl}^{mid} [r_{mid}, r_{out}], f_{cl}^{out} [r_{out}, r_{far}], f_{cl}^{far} ($>r_{far}$); see Fig. 2) for different winds regions derived by Puls et al. (2006). By using density-squared diagnostics, we can reproduce the emission flux at different wavelengths (wind regions) by adapting the corresponding clumping factor, since $F_\nu \propto \dot{M}\sqrt{f_{cl}}/R_\star$ is an invariant throughout the wind. By normalising clumping factors to the outermost wind region ($f_{cl}^{far} = 1$), we further derived the minimum radial stratification of the clumping factor through the stellar wind, $f_{cl}^{min}(r)$, and thus, the corresponding maximum mass-loss rate, $\dot{M}_{max}$.

Then, we compared our empirical $\dot{M}_{max}$ to the theoretical predictions by V00 and V01 ($\dot{M}_{th}^{Vink}$) as they are used in the often-cited grids of evolutionary models in codes such as Geneva (Ekström et al. 2012, Yusof et al. 2013), Bonn (e.g. Brott et al. 2011, Köhler et al 2015) and MESA (Modules for Experiments in Stellar Astrophysics; Paxton et al. 2011). V00 and V01 provide simple recipes to estimate $\dot{M}_{th}^{Vink}$ for various ranges of effective temperatures, depending on the so-called first and second `bi-stability jumps', where T_{eff}^{jump1} and T_{eff}^{jump2} depend on the mean wind density.

Geneva code uses the definitions of T_{eff}^{jump1} and T_{eff}^{jump2} from V00 and V01 ($T_{eff}^{jump1} = 27.5 - 22.5\,kK$, $T_{eff}^{jump2} \sim 18.5 - 12.5\,kK$; Geneva approach). In Bonn code and MESA T_{eff}^{jump1} is obtained as a function of the density of the wind via metallicity (V01; $T_{eff}^{jump1} = 27.5 - 22.5\,kK$) and T_{eff}^{jump2} is set to 10 kK (MESA approach). Finally, to investigate $\dot{M}_{th}^{Vink}$ as a function of a lower T_{eff}^{jump1} reported by several authors (e.g. Petrov et al. 2014), we carried out a third test, following the MESA implementation but fixing also T_{eff}^{jump1}(T_{eff}^{jump1} = 22 kK and T_{eff}^{jump2} = 10 kK; Fixed-jumps approach). See Figures 4 and 5.

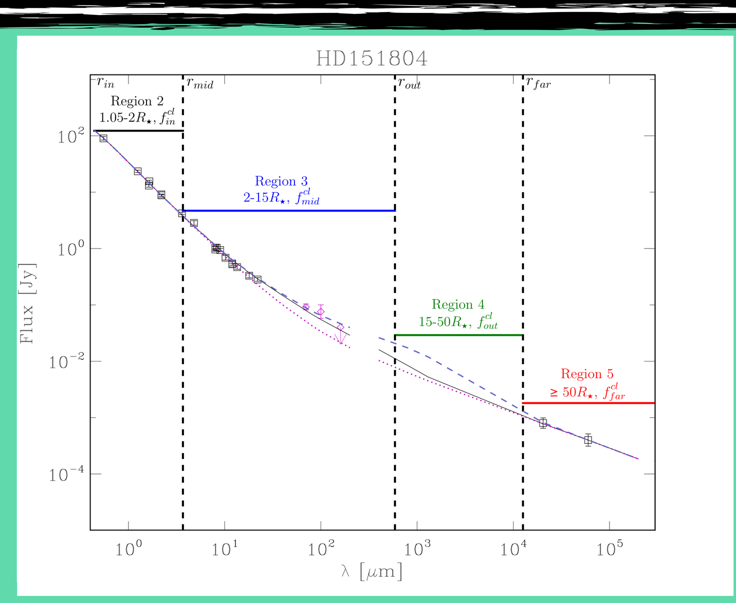

Figure 2. Observed and best-fit fluxes vs. wavelength for the O Supergiant HD 151804, and schematic of the defined clumping factors and wind regions as a function of the spectral range and their corresponding radial distance to the photosphere (r). Solid line corresponds to the best-fit model; magenta-dotted and blue-dashed lines correspond to different models. Magenta diamonds are our measured far-infrared fluxes at 70, 100 and 160 µm. Black squares indicate flux values from the literature. Plot adapted from Rubio-Díez et al. (2022).

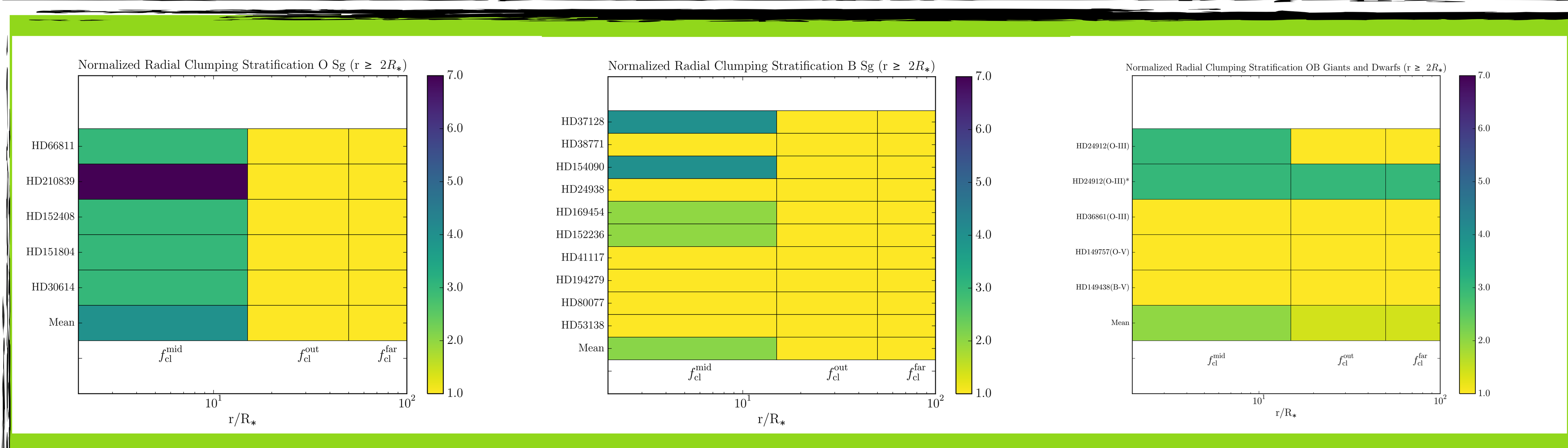

Figure 3.- From left to right: individual minimum and average values of the clumping factors for $r \gtrsim 2R_\star$ derived in this work for the sub-sample of O (left) and B (middle) supergiants , and OB dwarfs and giants (right). The binaries and non-thermal sources in our sample were removed prior to analyse the average clumping stratification.

Results.- Minimum Clumping Structure

I. The stellar wind at $r \gtrsim 2R_\star$ for most of the stars in our sample fulfills the clumping stratification condition $f_{cl}^{mid} \gtrsim f_{cl}^{out} \gtrapprox f_{cl}^{far} = f_{cl}^{min}$, regardless of the strength of the wind. The exceptions correspond to non-thermal or variable thermal sources in our sample.

II. The clumping-degree drop from the intermediate (f_{cl}^{mid}) to the outer wind region (f_{cl}^{out}) depends on spectral type and luminosity class: on average, f_{cl}^{mid} is ≈4 times larger than f_{cl}^{out} for O Supergiants (Fig.3-left), ≈2 times larger for B supergiants (Fig.3-middle) and similar to f_{cl}^{out} for OB dwarfs and giants (Fig.3-right).

III. Our findings agree well with the empirical clumping properties at $r \gtrsim 2R_\star$ derived by Najarro et al. (2011) and Clark et al. (2012) following a different parametrisation. In addition, our results overall support the hydrodynamical O Supergiants models by Sundqvist et al. (2013), and, tentatively, the recent 1D LDI simulations of OB Supergiants winds by Driessen et al. (2019), which predict lower amounts of clumping in B supergiants.

IV. We found that for 8 OB supergiants in our sample $f_{cl}^{in} > f_{cl}^{mid}$. This significantly extends the findings of Puls et al. (2006) in just one star of their sample (ζ Pup, HD 66811) and is in agreement with the empirical clumping properties by Najarro et al. (2011) and the theoretical predictions for O supergiants by Sundqvist et al. (2011, 2013). This suggests that such a behaviour, rather than being an exception, could imply the existence of two trends characterised by different physical conditions at the base of the wind.

Results.- Empirical maximum vs theoretical mass-loss rates for OB Supergiants throughout bi-stability jumps

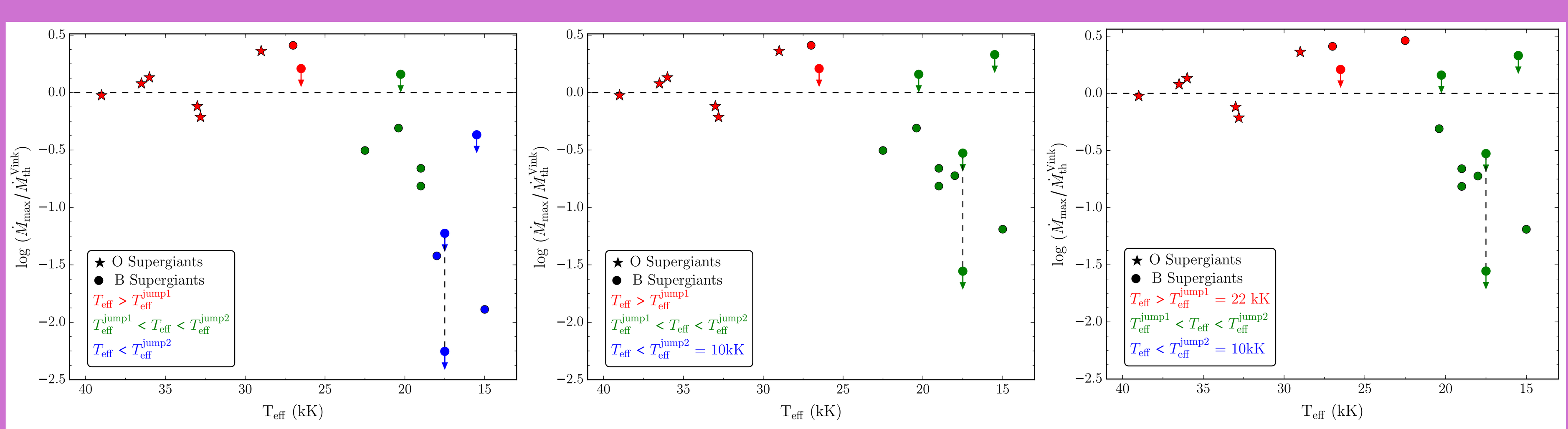

Figure 4. Empirical to theoretical mass-loss rates ratio, in logarithmic scale, as a function of effective temperature for the OB supergiants sub-sample. Empirical mass-loss rates correspond to the $\dot{M}_{max}$ derived in this work. Theoretical mass-loss rates, $\dot{M}_{th}^{Vink}$ correspond to the mass-loss rates computed via recipes from V00 and V01 for different definitions of the temperatures of the jumps (see Sec. Methods); ***left:*** *Geneva approach, middle: MESA approach, and* ***right:*** *Fixed-jumps approach. Different colours indicate at which side of the bi-stability jumps the sources are located. Arrows indicates upper limits and values joined by a dotted line are two possible solutions for a given source.*

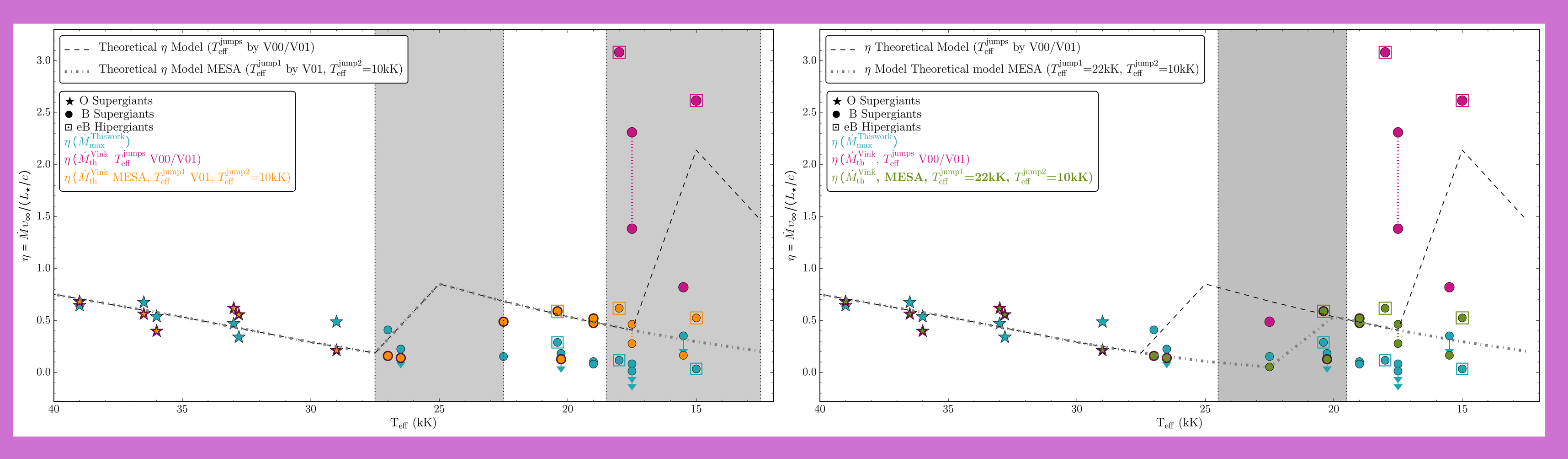

Figure 5. Empirical-maximum and theoretical wind performance numbers, $\eta = \dot{M}v_\infty/(L_\star/c)$, as a function of T_{eff}, for our OB supergiants sub-sample. ***Left:*** *Empirical estimates (clear blue) vs. Geneva (magenta) and MESA (orange) approaches. Dashed and dotted-dashed lines correspond to theoretical predictions for a source with $\log L_\star/L_\odot = 5.75$ and $M_\star = 45M_\odot$ for solar metallicity, respectively, based on Geneva and MESA implementations of V00 and V01 (see Sec. Methods).* ***Right:*** *Same as left panel, but showing theoretical η in the Geneva (magenta) and Fixed-jumps (light green) approaches, and a dotted-dashed line marking the theoretical model based on the Fixed-jumps temperatures implementations of V00 and V01 (see Sec. Methods).*
The shadowed regions represents the first and second bi-stability jump zones as defined by V00 (left-panel) and observations (e.g. Lamers et al. 1995, Markova & Puls 2008; right-panel). For symbols and color code see legends; arrows and dotted lines as in Fig. 4.

V. For O supergiants the derived upper-limit mass-loss rates, $\dot{M}_{max}$, agree with the theoretical predictions by V00 and V01 for unclumped winds, whereas B supergiants show a discrepancy which severely increases with decreasing effective temperature: $\dot{M}_{max}$ starts to differ from theoretical recipes in the predicted first bi-stability transition zone, and up to 1.5-2 orders of magnitude lower for the coolest B supergiants below the first bi-stability jump (Fig. 4). Since the empirical scaling invariant is $\sim \dot{M}\sqrt{f_{cl}}$ and our derived mass-loss rates are upper limits assuming an unclumped radio-emitting wind ($f_{cl} = f_{cl}^{far} = 1$), any clumping in this outermost region would only increase this discrepancy.

VI. The $\dot{M}_{max}$ values derived in this work agree (on average) with others obtained by various studies present in the literature (e.g. Crowther et al. 2006, Haucke et at. 2018), by means of H_α fitting using unclumped wind models, and with recent theoretical mass-loss estimates for O supergiants (Björklund et al. 2021).

VII. We find that the wind-performance number, η, for our sample (Fig. 5) shows a gradually decreasing trend –albeit again with significant scatter– with decreasing T$_{eff}$ and there is no evidence for sudden increases (Vink et al. 1999, V00 and V01), or a secondary local maximum, at any of the predicted bi-stability limits. This is quite similar to the findings by e.g. Benaglia et al. (2007), Markova & Puls (2008) and Haucke et al. (2018).

Conclusions.-

Take a look at the paper!

A key conclusion of our analysis regards the upper-limit mass-loss rates of OB supergiants derived from radio emission. Although the actual empirical $\dot{M}$ will depend on the level of clumping in the outermost wind, these upper limits should be quite robust since radio emission is a relatively 'clean' diagnostic. If the absolute value of clumping in the outermost wind region of OB supergiants was $f_{cl}^{far} = 4 - 9$ as suggested by the hydrodynamic O-star models by Runacres et al. (2002, 2005), the theoretical mass-loss rate recipes by Vink et al. (2000, 2001) would be overestimated by a factor 2 - 3 for O supergiants; this would then agree well with the recent theoretical O-star mass-loss predictions by Björklund et al. (2021). On the other hand, the consequences for B supergiants across the bi-stability regions are dramatically independent of their clumping properties, and temperatures of the jumps, since these objects require downward $\dot{M}_{th}^{Vink}$ corrections of up to 1.5 - 2 orders of magnitude, even in the case in which B supergiants were not as clumped as O supergiants (Driessenet al. 2019). Thus, this finding calls for an urgent re-investigation of the role recombination of iron-like elements plays in determining the mass-loss rates of objects that cross the bi-stability region, as well as a careful analysis of corresponding effects for stellar evolution models.